ISA Transactions 80 (2018) 491–502

Contents lists available at ScienceDirect

ISA Transactions

journal homepage: www.elsevier.com/locate/isatrans

Research article

Multi-objective control for cooperative payload transport with rotorcraft UAVs

Javier Gimenez*, Daniel C. Gandolfo, Lucio R. Salinas, Claudio Rosales, Ricardo Carelli

Instituto de Automática, Universidad Nacional de San Juan-CONICET, Argentina

ARTICLE INFO

Keywords:
Cooperative transport
Rotorcraft UAV
Multi-objective control
Null-space
Lyapunov theory

ABSTRACT

A novel kinematic formation controller based on null-space theory is proposed to transport a cable-suspended payload with two rotorcraft UAVs considering collision avoidance, wind perturbations, and properly distribution of the load weight. An accurate 6-DoF nonlinear dynamic model of a helicopter and models for flexible cables and payload are included to test the proposal in a realistic scenario. System stability is demonstrated using Lyapunov theory and several simulation results show the good performance of the approach.

1. Introduction

Due to its superior mobility in a three-dimensional space, the use of unmanned aerial vehicles for load manipulation is gaining support in several applications and attracting the attention of many researchers. Significant focus has been placed on unmanned rotorcraft systems because of their capacities to move in all directions, fly at low speed, hover, take off and land vertically in small spaces and under challenging topography conditions.

Conventional methods require an immense effort to deliver certain payloads, for which aerial transport is the only solution in many cases. There are several air transport applications including supplying medicines and food, precise spraying in agriculture, carrying water for fighting forest fires, moving construction material, transferring loads between ships, rescuing humans in remote areas, among other tasks [1,2]. Many applications require the transportation of a heavy payload, and for them, the use of more than one UAV is a more convenient (or the only) solution. Flexible cables are generally used since they do not require to carry manipulators or grippers onboard the rotorcraft allowing to transport heavier objects. In addition, cables with longer extension can be used to conform cooperative formations with greater degrees of freedom. Furthermore, in this way, the payload can be protected from the propeller wash due to its distance to them [3,4].

Multi-Vehicle cooperative control for flying with a suspended load is a challenging and hazardous task since the load changes significantly the flight characteristics of the aerial vehicles. Control strategy of this formation structure is a hard issue due to the suspended payload is a swinging pendulum [5]. The presence of no-fly zones and obstacles are other complications for the control of this type of formations [6].

1.1. Related works

Several approaches for air transport using UAVs have been reported in the bibliography. In Ref. [7] the authors propose a nonlinear $\mathscr{H}_\infty$ robust controller to solve the payload transportation problem by using a quadrotor UAV along a predefined trajectory. For the transportation of cable-suspended loads, an iLQR optimal controller for quadrotor is presented in Refs. [8] and [9]. The lift maneuver problem and payload position control using a nonlinear geometric controller are addressed in Refs. [10,11]. The authors in Ref. [12] explore the transportation capability of an aerial manipulator to carry a heavy load using motion generation based on inverse kinematics. These approaches have interesting and validated results, but a single UAV is used and the payload weight is limited.

On the other hand, many authors have approached the problematic of cooperative aerial transport using two or more UAVs. A kinematic cooperative control for payload positioning through multiple aerial robots with cables is dealt in Ref. [13], and an asymptotically stable analytic algorithm based on dialytic elimination is proposed. A configuration of multiple robots that ensure static equilibrium of the payload at a desired 3D pose is presented in Ref. [14], demonstrating the good performance via simulation and experimental results. A geometric controller is proposed in Ref. [15] so that a rigid body payload can asymptotically follow a desired trajectory in presence of uncertainties. A cooperative control system for aerial robots to carry hoses by using particle swarm optimization theory for PID tuning is presented in Ref. [16]. All the above mentioned references present interesting approaches but perturbations (as wind) are not considered.

The authors in Refs. [17] and [18] consider the problem in presence

* Corresponding author.
E-mail address: jgimenez@inaut.unsj.edu.ar (J. Gimenez).

https://doi.org/10.1016/j.isatra.2018.05.022
Received 4 December 2017; Received in revised form 26 April 2018; Accepted 26 May 2018
Available online 01 June 2018

of parametric uncertainties and external disturbances such as wind. In both cases, robust controllers are proposed by using adaptive fuzzy theory and Lyapunov technique respectively, but collision avoidance is not addressed. Planning and control of multiple aerial robots manipulating and carrying a payload is proposed in Ref. [19], and two quality measures are considered for motion plan design minimizing individual robot motion and maximizing payload stability. A multi-UAV distributed architecture that allows different levels of cooperation and coordination among UAVs and between the UAVs and the environment are presented in Ref. [20]. This approach performs trajectory planning enabling the payload to navigate through safe areas, but again, the obstacle avoidance is not considered.

Unlike ground vehicles, the UAVs never stop consuming energy, because they must keep itself and the load in the air all the time. This is even more critical in rotary-wing UAVs where the lift phenomenon is not produced (as in fixed-wing UAVs) and the thrust must be fully generated by the propulsion system (see Ref. [21] for more details). Based on this, onboard energy availability is strongly influenced by the transported weight. This critical and very frequent situation is not considered by the aforementioned approaches for air transport. In this paper, the distribution of load weight for each UAV can be set and changed at any time while the mission is running according to onboard energy availabilities or load capabilities.

1.2. The proposal

In this paper, a novel kinematic formation controller based on null-space theory [22] is proposed in order for a payload hanging through flexible cables from two rotorcraft UAVs to follow a desired trajectory. Both the wind disturbance and the obstacle avoidance are taken into account in this control proposal. Then, the control objectives in this approach are: a) the payload must follow a desired trajectory compensating oscillations produced by external factors such as wind; b) the formation must avoid obstacles; c) The distance between the UAVs must be within a predetermined safety distance range; d) The UAVs must regulate their altitude to properly distribute the load weight between them; and e) The formation must navigate tangentially to the desired trajectory to avoid payload oscillations caused by frontal accelerations in the transportation. Besides, all these tasks are carried out simultaneously avoiding as many conflicts between them as possible.

While there are several multi-objective works in robotics addressed with the null-space theory [22], the cooperative payload transportation presents additional difficulties that do not allow the straightforward application of the technique. The main problem comes from the fact that the load can not be directly operated, but only through the vehicles. This considerably reduces the degrees of freedom, which must be used optimally to navigate safely, and at the same time, transport the load in the desired way. Overcoming these complications requires a thorough study of the compatibilities between tasks and a complex priority design that favors the fulfillment of as many objectives as possible. In the paper, two ways to avoid conflicts between tasks are proposed. One is to place conflicting tasks on the same priority level, even if this implies modifying the logical order of priorities. Another is to calculate the control action necessary to fulfill the less priority tasks under the assumption that the highest priority tasks are always fulfilled.

Finally, the outputs of the proposed kinematic controller can be coupled with a dynamic model of any rotorcraft UAV through an adaptation stage to obtain the control actions necessary to reach the kinematic references. In this paper, a very accurate dynamic model of a mini-helicopter [23] and a model for the load are considered to evaluate and validate the control strategy in a real test scenario.

The paper is organized as follows. The problem is formulated in Section 2. The task variables necessary to characterize the problem and the corresponding Jacobians are presented in Section 3. The control objectives with their respective priorities and conflicts, and the null-space based controller with a stability analysis are developed in Section 4. Section 5 presents the dynamic models of the helicopters and the load used to test the kinematic controller. Simulations are shown in Section 6 and conclusion are drawn in Section 7.

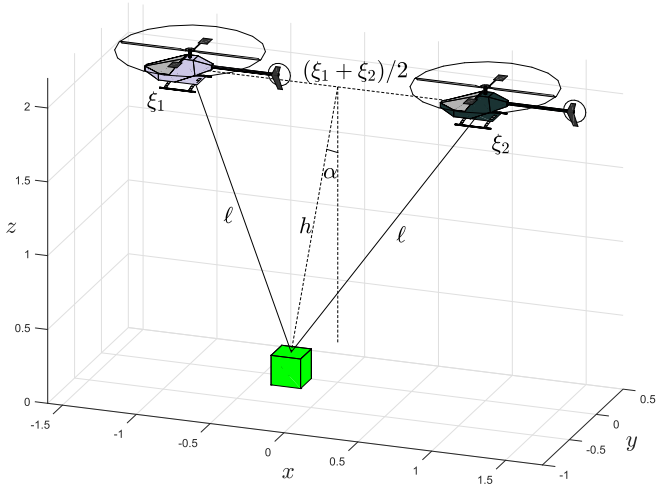

Fig. 1. Geometry of the problem.

2. Problem formulation

Consider two rotorcraft UAVs cooperatively carrying a cable-suspended payload. Let ξ_1 and ξ_2 be the vehicle positions, where $\xi_i = [x_i, y_i, z_i]^T$ coincides with the gravity center (g.c.) of the i-th vehicle. In addition, their orientations are denoted with ψ_1 and ψ_2 respectively. In this paper, the system configuration is given by $\mathbf{q} = [\xi_1^T, \psi_1, \xi_2^T, \psi_2]^T$.

Consider that there are two cables of length ℓ that join the vehicles with a point-mass payload. Suppose the load performs pendular movements on the plane perpendicular to the virtual segment that joins the two vehicles and passes through the point $(\xi_1 + \xi_2)/2$ (see dashed lines in Fig. 1). In practice, the payload may not be in the mentioned plane due to elasticity and deformation of the cables. However, these effects are assumed negligible for simplicity. The load forms an angle α with the plane perpendicular to the x-y plane that contains the aforementioned segment (see Fig. 1).

The formation must fulfill a number of tasks sorted according to the following priorities:

1) Obstacles avoidance is the highest priority task.
2) The secondary objectives are:
   - 2.1) Safety distances between vehicles: These must be in a predetermined range to avoid collisions or undesirable separation.
   - 2.2) Properly distribution of the load weight between the vehicles: The evenly distribution of the load or the load distribution according to the vehicle capacities are desirable issues.
   - 2.3) Trajectory tracking in z for the payload: Placing tasks 2.2 and 2.3 at the same level is essential to coordinate the heights of the vehicles in order to satisfy both tasks simultaneously.
3) The payload must to follow a predetermined trajectory in x-y to reduce oscillations caused by external factors such as wind.
4) The formation must to navigate tangentially to the path curve avoiding load oscillations caused by frontal acceleration of the vehicles.

The priority order in which tasks are performed establishes which one of them can be omitted in critical situations. For more details see Sections 4.1 and 4.2.

Based on null-space theory, this paper proposes kinematic velocities $\mathbf{v}_c$ for the configuration variables $\mathbf{q}$ necessary to fulfill as many tasks as

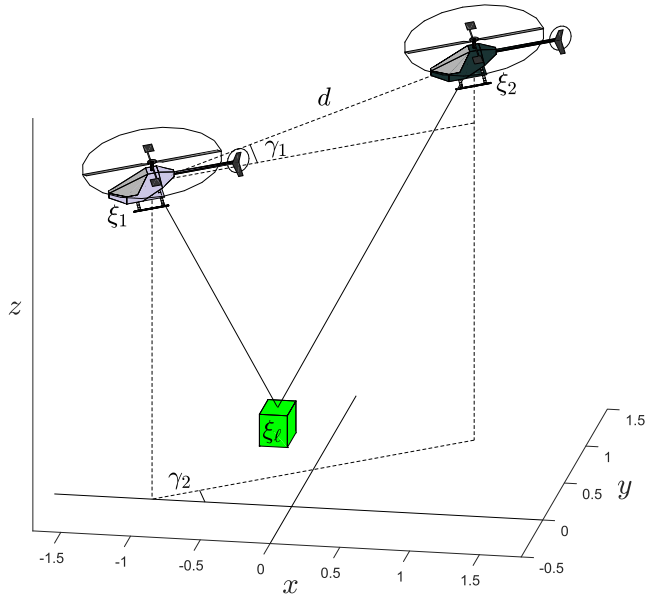

Fig. 2. Posture of the formation.

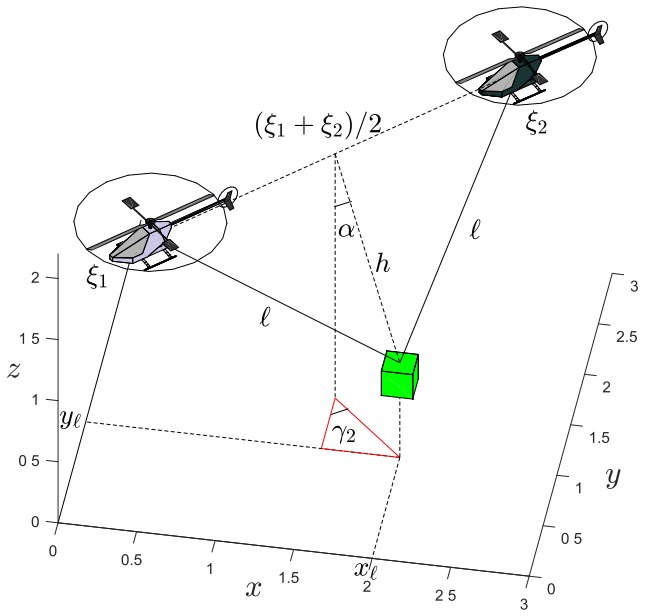

Fig. 3. Geometry of the load position.

possible, and subsequently, the control actions necessary to reach these velocities are provided in an external loop.

3. Task variables and their Jacobians

Task variables are quantities that characterize directly the tasks to fulfill, and whose derivatives are linearly related to $\dot{\mathbf{q}}$ through Jacobians. The relation between configuration and task variables allows the straightforward definition of the kinematic controller $\mathbf{v}_c$. This section presents the task variables and their respective Jacobians, which are classified in four groups: formation, payload, obstacle avoidance, and orientation variables.

For simplicity, for all angle β, the notations s_β and c_β are used to represent sin β and cos β respectively.

3.1. Formation variables

The formation is determined by the following variables (see Fig. 2): the distance between the vehicles

$$d = \|\xi_1 - \xi_2\|,$$

and the orientation angles of the virtual segment that links them

$$\gamma_1 = \text{asin}\left(\frac{z_2 - z_1}{d}\right), \text{ and } \gamma_2 = \text{atan}\left(\frac{y_2 - y_1}{x_2 - x_1}\right).$$

Their time derivatives are given by

$$\dot{d} = \frac{(\xi_1 - \xi_2)^T(\dot{\xi}_1 - \dot{\xi}_2)}{d} = \mathbf{J}_d\dot{\mathbf{q}}, \tag{1}$$

$$\dot{\gamma}_1 = \frac{(\dot{z}_2 - \dot{z}_1)d - (z_2 - z_1)\dot{d}}{d\sqrt{d^2 - (z_2 - z_1)^2}} = \mathbf{J}_{\gamma_1}\dot{\mathbf{q}}, \tag{2}$$

$$\dot{\gamma}_2 = \frac{(x_2 - x_1)(\dot{y}_2 - \dot{y}_1) - (\dot{x}_2 - \dot{x}_1)(y_2 - y_1)}{(x_2 - x_1)^2 + (y_2 - y_1)^2} = \mathbf{J}_{\gamma_2}\dot{\mathbf{q}}, \tag{3}$$

where

$$\mathbf{J}_d = \mathbf{J}_d(\mathbf{q}) = \frac{1}{d}[x_1 - x_2 \;\; y_1 - y_2 \;\; z_1 - z_2 \;\; 0 \;\; x_2 - x_1 \;\; y_2 - y_1 \;\; z_2 - z_1 \;\; 0],$$

$$\mathbf{J}_{\gamma_1} = \mathbf{J}_{\gamma_1}(\mathbf{q}) = \frac{1}{\sqrt{d^2 - (z_2 - z_1)^2}}[0 \;\; 0 \;\; -1 \;\; 0 \;\; 0 \;\; 0 \;\; 1 \;\; 0] + \frac{z_1 - z_2}{d\sqrt{d^2 - (z_2 - z_1)^2}}\mathbf{J}_d,$$

$$\mathbf{J}_{\gamma_2} = \mathbf{J}_{\gamma_2}(\mathbf{q}) = \frac{1}{(x_2 - x_1)^2 + (y_2 - y_1)^2} \times [y_2 - y_1 \;\; x_1 - x_2 \;\; 0 \;\; 0 \;\; y_1 - y_2 \;\; x_2 - x_1 \;\; 0 \;\; 0].$$

3.2. Payload variables

The payload position $\xi_\ell = [x_\ell, y_\ell, z_\ell]^T$ is another variable of interest. If both vehicles fly at the same altitude ($\gamma_1 = 0$), then

$$\xi_\ell = \frac{\xi_1 + \xi_2}{2} + h\begin{bmatrix} s_\alpha s_{\gamma_2} \\ -s_\alpha c_{\gamma_2} \\ -c_\alpha \end{bmatrix}, \tag{4}$$

with $h = h(\mathbf{q}) = \sqrt{\ell^2 - d^2/4}$ (see Fig. 3). When $\gamma_1 \neq 0$, it is assumed that the payload position is also calculated according to (4). This practical assumption avoids conflicts between tasks and introduces negligible errors (see Section 4.1 for more details).

The payload velocity is given by

$$\dot{\xi}_\ell = \frac{\dot{\xi}_1 + \dot{\xi}_2}{2} + \frac{d}{4h}\begin{bmatrix} s_\alpha s_{\gamma_2} \\ -s_\alpha c_{\gamma_2} \\ -c_\alpha \end{bmatrix}\dot{d} + hs_\alpha\begin{bmatrix} c_{\gamma_2} \\ s_{\gamma_2} \\ 0 \end{bmatrix}\dot{\gamma}_2 + h\begin{bmatrix} c_\alpha s_{\gamma_2} \\ -c_\alpha c_{\gamma_2} \\ s_\alpha \end{bmatrix}\dot{\alpha} = \mathbf{J}_\ell\dot{\mathbf{q}} + \mathbf{A}_\ell, \tag{5}$$

where

$$\mathbf{J}_\ell = \begin{bmatrix} \mathbf{J}_{\ell,x} \\ \mathbf{J}_{\ell,y} \\ \mathbf{J}_{\ell,z} \end{bmatrix} = \mathbf{J}_\ell(\mathbf{q}, \alpha) = \frac{1}{2}[\mathbf{I}_3 \;\; \mathbf{0}_{3\times1} \;\; \mathbf{I}_3 \;\; \mathbf{0}_{3\times1}] + \frac{d}{4h}\begin{bmatrix} s_\alpha s_{\gamma_2} \\ -s_\alpha c_{\gamma_2} \\ -c_\alpha \end{bmatrix}\mathbf{J}_d + hs_\alpha\begin{bmatrix} c_{\gamma_2} \\ s_{\gamma_2} \\ 0 \end{bmatrix}\mathbf{J}_{\gamma_2},$$

$$\mathbf{A}_\ell = \begin{bmatrix} A_{\ell,x} \\ A_{\ell,y} \\ A_{\ell,z} \end{bmatrix} = \mathbf{A}_\ell(\mathbf{q}, \alpha, \dot{\alpha}) = h\begin{bmatrix} c_\alpha s_{\gamma_2} \\ -c_\alpha c_{\gamma_2} \\ s_\alpha \end{bmatrix}\dot{\alpha}.$$

3.3. Variable of obstacle avoidance

Consider that in the working environment there are N dynamic obstacles with positions $\xi_{o,i} = \xi_{o,i}(t) = [x_{o,i}(t), y_{o,i}(t), z_{o,i}(t)]^T$, $1 \leq i \leq N$. Taking into account the formation type, the vehicles should navigate in a cooperative way avoiding these obstacles. For this purpose, the formation center is defined as

$$\xi_c = \begin{bmatrix} x_c \\ y_c \\ z_c \end{bmatrix} = \frac{\xi_1 + \xi_2 + \xi_\ell}{3},$$

whose time derivative is given by

$$\dot{\xi}_c = \frac{\dot{\xi}_1 + \dot{\xi}_2 + \dot{\xi}_\ell}{3} = \frac{1}{3}(\mathbf{J}_\ell + [\mathbf{I}_3 \;\; \mathbf{0}_{3\times 1} \;\; \mathbf{I}_3 \;\; \mathbf{0}_{3\times 1}])\dot{\mathbf{q}} + \frac{1}{3}\mathbf{A}_\ell.$$

Each obstacle has a repulsion zone determined by a potential field given by

$$\begin{aligned} V_i &= V_i(\mathbf{q}, \alpha, \xi_{o,i}) \\ &= \exp\left\{-\frac{(x_c - x_{o,i})^n}{a_x} - \frac{(y_c - y_{o,i})^n}{a_y} - \frac{(z_c - z_{o,i})^n}{a_z}\right\}, \end{aligned} \tag{6}$$

where $a_x > 0$, $a_y > 0$, $a_z > 0$ and $n > 0$ (even number) are design parameters. Note that V_i depends on α because ξ_c depends on ξ_ℓ, which in turn depends on α. A small threshold $\varsigma > 0$ is defined for V_i from which the corresponding obstacle is considered to be close. This assumption is necessary since the null space technique requires that $V_i = 0$ in order to address the less priority tasks. For this reason, it is considered $V_i = 0$ if $V_i < \varsigma$.

Then, when the formation is close to the i-th obstacle ($V_i \geq \varsigma$), it results

$$\begin{aligned} \dot{V}_i &= V_i\left(-\frac{n(x_c - x_{o,i})^{n-1}}{a_x}(\dot{x}_c - \dot{x}_{o,i})\right. \\ &\quad \left. - \frac{n(y_c - y_{o,i})^{n-1}}{a_y}(\dot{y}_c - \dot{y}_{o,i}) - -\frac{n(z_c - z_{o,i})^{n-1}}{a_z}(\dot{z}_c - \dot{z}_{o,i})\right) \\ &= \mathbf{J}_{V_i}\dot{\mathbf{q}} + \mathbf{A}_{V_i}, \end{aligned} \tag{7}$$

where

$$\mathbf{J}_{V_i} = \mathbf{J}_{V_i}(\mathbf{q}, \alpha, \xi_{o,i}) = -\frac{1}{3}\mathbf{a}_i^T(\mathbf{J}_\ell + [\mathbf{I}_3 \;\; \mathbf{0}_{3\times 1} \;\; \mathbf{I}_3 \;\; \mathbf{0}_{3\times 1}]),$$

$$\mathbf{A}_{V_i} = \mathbf{A}_{V_i}(\mathbf{q}, \alpha, \dot{\alpha}, \xi_{o,i}, \dot{\xi}_{o,i}) = \mathbf{a}_i^T\left(\dot{\xi}_{o,i} - \frac{1}{3}\mathbf{A}_\ell\right),$$

with

$$\mathbf{a}_i = \mathbf{a}_i(\mathbf{q}, \alpha, \xi_{o,i}) = nV_i\begin{bmatrix} \frac{(x_c - x_{o,i})^{n-1}}{a_x} \\ \frac{(y_c - y_{o,i})^{n-1}}{a_y} \\ \frac{(z_c - z_{o,i})^{n-1}}{a_z} \end{bmatrix}.$$

Then, the variable of the obstacle avoidance is the total potential field of the obstacles defined by

$$V = V(\mathbf{q}, \alpha, \{\xi_{o,i}\}) = \sum_{i=1}^{N} V_i,$$

with

$$\dot{V} = \mathbf{J}_V\dot{\mathbf{q}} + \mathbf{A}_V, \tag{8}$$

where

$$\mathbf{J}_V = \mathbf{J}_V(\mathbf{q}, \alpha, \{\xi_{o,i}\}) = \sum_{i=1}^{N} \mathbf{J}_{V_i},$$

and

$$\mathbf{A}_V = \mathbf{A}_V(\mathbf{q}, \alpha, \dot{\alpha}, \{\xi_{o,i}\}, \{\dot{\xi}_{o,i}\}) = \sum_{i=1}^{N} \mathbf{A}_{V_i}.$$

3.4. Orientation variables

Finally, the orientation variables are the vehicle orientations ψ_1 and ψ_2, whose associated Jacobians are given by

$$\mathbf{J}_{\psi_1} = [0 \;\; 0 \;\; 0 \;\; 1 \;\; 0 \;\; 0 \;\;\; 0],$$

$$\mathbf{J}_{\psi_2} = [0 \;\; 0 \;\; 0 \;\; 0 \;\; 0 \;\; 0 \;\; 0 \;\; 1].$$

4. Kinematic formation controller

The kinematic velocities $\mathbf{v}_c$ of the vector state $\mathbf{q}$ required to fulfill the predefined tasks and their priorities are found in this Section. A controller based on null-space [22] is used to this end. This controller has a geometric deduction and works projecting desired velocities of lower priority tasks on the null-space of the Jacobian of the higher priority tasks.

There is a conflict between tasks when they can not be simultaneously verified. The definition of the task variables, the priorities between tasks, and the control objectives are key issues to avoid as many conflicts between tasks as possible. The under-actuated characteristic of the system requires a meticulous and complex definition of these settings. This section presents a novel setting that allows to perform the tasks simultaneously when there are no obstacles nearby.

4.1. Control objectives and their priorities

The first objective is the obstacle avoidance for which the ideal situation is to navigate in zones where $V = 0$. When entering in an obstacle zone ($V_i \geq \varsigma$ for any i), it is also desired that $\dot{V} = 0$ in order to avoid obstacles by navigating through the level curves of V. Consider the velocity vector

$$\mathbf{v}_c^{(1)} = \mathbf{J}_1^\dagger(-k_V V - \mathbf{A}_V), \tag{9}$$

where $\mathbf{J}_1 = \mathbf{J}_1(\mathbf{q}, \alpha, \{\xi_{o,i}\}) = \mathbf{J}_V$ is the Jacobian of task 1, the superscript $\dagger$ represents the pseudoinverse matrix, and $k_V > 0$ is a design constant. This velocity vector satisfies task 1 (see Section 4.3). The set of desired velocity vectors for which it is possible to perform the first task is conformed by the vectors of the form

$$\mathbf{v} = \mathbf{v}_c^{(1)} + (\mathbf{I}_8 - \mathbf{J}_1^\dagger\mathbf{J}_1)\mathbf{w}, \quad \mathbf{w} \in IR^8, \tag{10}$$

since $\mathbf{J}_1\mathbf{v} = \mathbf{J}_1\mathbf{v}_c^{(1)}$. Among all of them, the minimum norm solution is $\mathbf{v}_c^{(1)}$.

Note that $(\mathbf{I}_8 - \mathbf{J}_1^\dagger\mathbf{J}_1)\mathbf{w}$ is the orthogonal projection of $\mathbf{w}$ on the null space of $\mathbf{J}_1$ denoted by $\mathcal{N}(J_1)$. From here on, the minimum norm velocities defined to fulfill the other tasks are projected on the null space of the Jacobians of the higher-priority tasks, so as not to compromise their fulfillment. These projections modify the required velocities if they compromise the fulfillment of the higher-priority tasks, that is, if this velocity vector is not in the null space of the Jacobians of the higher-priority tasks. These modifications compromise the fulfillment of the lower-priority tasks, and for this, strategies that produce non-conflicting minimum norm solutions should be sought. One of these strategies consists in calculating the Jacobians corresponding to the lower-priority tasks assuming that the higher-priority tasks are fulfilled or under ideal and practical assumptions. This is why (4) and (5) were calculated assuming that $\gamma_1 \approx 0$.

Placing conflicting tasks at the same priority level can avoid the conflict among them. Usually, there are velocities that satisfy two tasks at the same time, and others that satisfy only one of them. If both tasks have the same priority, the minimum norm solution (if it exists) is a velocity vector that satisfies both tasks. But if task 1 has higher priority

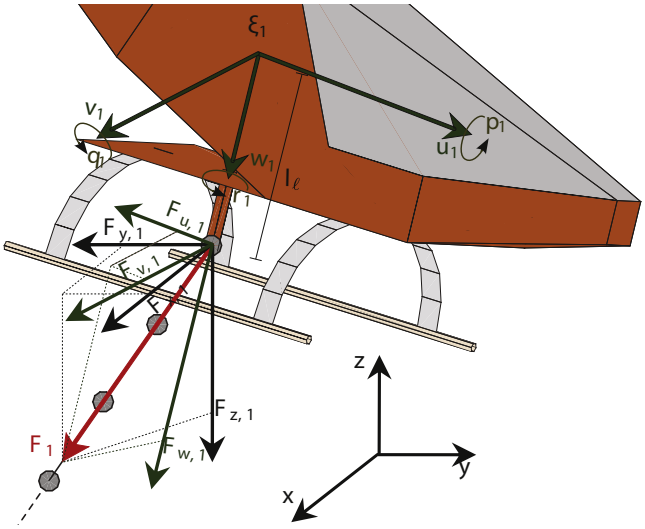

Fig. 4. Graphical representation of the mini-helicopter N°1 and cable connection point (spherical joint) below the helicopter g.c. (ξ_1). The load force (F_1) is expressed in two coordinate systems: inertial axes $\langle x, y, z\rangle$ and helicopter's body axes $\langle u_1, v_1, w_1\rangle$.

than task 2, the minimum norm solution for task 2 may not satisfy task 1. Then, this solution is modified by projecting it onto the null space of task 1, and this new velocity vector may not satisfy task 2.

The desired height for the load (in principle a tertiary objective) is optimally achieved through a combination of two operations: modifying the altitude of the vehicles and adjusting the distance between them. By projecting the resulting desired velocity on $\mathcal{N}(\mathbf{J}_d)$ (secondary objective), the second operation is canceled and a steady state error in the payload height is produced. To solve this conflict, both tasks are considered secondary objectives. Thus, the second objective is the properly distribution of the load weight maintaining a safety distance $d_m \le d \le d_M$ between them while the load remains at a desired height $z_\ell(t) = z^*(t)$.

The load weight produces a force F_i with norm f_i on each vehicle (see Fig. 4), which are noisy by nature. In order to generate smooth control actions, a low-pass filtered version $\breve{f}_i$ of these signals should be incorporated in the control loop. A mean filtering with sliding-window is used in this paper.

If both vehicles navigate at the same altitude ($\gamma_1 = 0$), the vehicle ahead makes a major effort (see Fig. 5). The vehicle that is behind must navigate a little higher to compensate for this situation. This idea can be

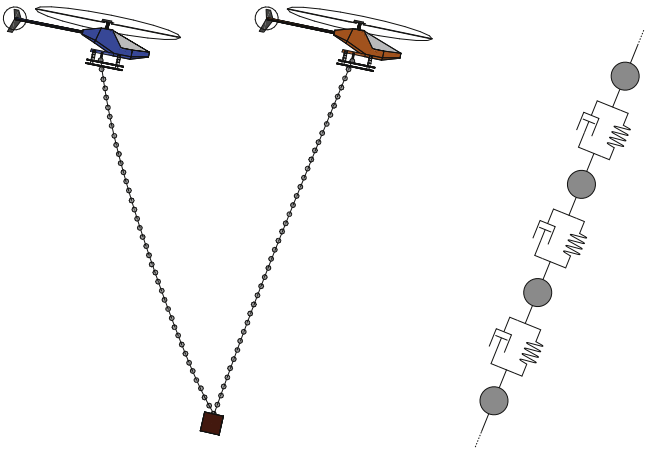

Fig. 5. Graphical representation of mini-helicopters carrying a cable-suspended payload (left) and cable section represented by mass-spring-damper systems (right).

extended so that the vehicles regulate their altitudes in order to transport proportions $(\rho, 1-\rho)$, $\rho \in (0, 1)$, of the load. Since the altitude difference is characterized by γ_1, its desired value is defined by

$$\gamma_{1,d} = \gamma_1 + k_{\gamma_1,1} \tanh\left(k_{\gamma_1,2}\left(\frac{\breve{f}_1}{\rho} - \frac{\breve{f}_2}{1-\rho}\right)\right),$$

with $k_{\gamma_1,1}, k_{\gamma_1,2} > 0$. Then, the control objective is $\widetilde{\gamma}_1(t) = \gamma_{1,d}(t) - \gamma_1(t) \to 0$. Note that ρ can be variable, and then, it includes potentialities such as being defined proportional to the onboard energy availability.

Regarding navigation maintaining a safety distance, it is defined

$$\widetilde{d} = \begin{cases} -k_{d,1}\tanh(k_{d,2}(d-d_m)) & \text{if } d < d_m, \\ 0 & \text{if } d_m \le d \le d_M, \\ -k_{d,1}\tanh(k_{d,2}(d-d_M)) & \text{if } d > d_M, \end{cases} \tag{11}$$

with $k_{d,1}, k_{d,2} > 0$. This produces control actions only when $d \notin [d_m, d_M]$ reducing as much as possible the time that the task is not satisfied.

Note that from (1), (2) and (5), it results

$$\begin{bmatrix} \dot{d} \\ \dot{\gamma}_1 \\ \dot{z}_\ell \end{bmatrix} = \mathbf{J}_2\dot{\mathbf{q}} + \mathbf{A}_2, \tag{12}$$

where

$$\mathbf{J}_2 = \mathbf{J}_2(\mathbf{q}, \alpha) = \begin{bmatrix} \mathbf{J}_d \\ \mathbf{J}_{\gamma_1} \\ \mathbf{J}_{\ell,z} \end{bmatrix}, \text{ and } \mathbf{A}_2 = \mathbf{A}_2(\mathbf{q}, \alpha, \dot{\alpha}) = \begin{bmatrix} 0 \\ 0 \\ A_{\ell,z} \end{bmatrix}.$$

The minimal norm control law to fulfill the second task is given by

$$\mathbf{v}_c^{(2)} = \mathbf{J}_2^\dagger \begin{bmatrix} \widetilde{d} \\ \dot{\gamma}_{1,d} + \widetilde{\gamma}_1 \\ \dot{z}^* - k_{\ell,z,1}\tanh(k_{\ell,z,2}(z_\ell - z^*)) - A_{\ell,z} \end{bmatrix}, \tag{13}$$

with $k_{\ell,z,1}, k_{\ell,z,2} > 0$.

If tasks 1 and 2 are compatible ($\mathbf{J}_2\mathbf{J}_1^\dagger = \mathbf{0}$), then $\mathbf{v}_c^{(2)} \in \mathcal{N}(\mathbf{J}_1)$ and both tasks can be satisfied at once by using

$$\mathbf{v}_c = \mathbf{v}_c^{(1)} + (\mathbf{I}_8 - \mathbf{J}_1^\dagger\mathbf{J}_1)\mathbf{v}_c^{(2)}, \tag{14}$$

since $\mathbf{J}_2\mathbf{v}_c = \mathbf{J}_2\mathbf{v}_c^{(2)}$. If tasks are not compatible, then task 2 will be not fulfilled, although it will be performed in the best possible way without conditioning task 1. Note that (14) is (10) with $\mathbf{w} = \mathbf{v}_c^{(2)}$. A detailed analysis of compatibility between the proposed control objectives is developed in Section 4.2.

The third objective requires the payload trajectory to verify $x_\ell(t) = x^*(t)$ and $y_\ell(t) = y^*(t)$. From (5), it results

$$\begin{bmatrix} \dot{x}_\ell \\ \dot{y}_\ell \end{bmatrix} = \mathbf{J}_3\dot{\mathbf{q}} + \mathbf{A}_3, \tag{15}$$

where

$$\mathbf{J}_3 = \mathbf{J}_3(\mathbf{q}, \alpha) = \begin{bmatrix} \mathbf{J}_{\ell,x} \\ \mathbf{J}_{\ell,y} \end{bmatrix}, \text{ and } \mathbf{A}_3 = \mathbf{A}_3(\mathbf{q}, \alpha, \dot{\alpha}) = \begin{bmatrix} A_{\ell,x} \\ A_{\ell,y} \end{bmatrix}.$$

Then, the minimal norm control law to fulfill the third task is given by

$$\mathbf{v}_c^{(3)} = \mathbf{J}_3^\dagger \begin{bmatrix} \dot{x}^* - k_{\ell,x,1}\tanh(k_{\ell,x,2}(x_\ell - x^*)) - A_{\ell,x} \\ \dot{y}^* - k_{\ell,y,1}\tanh(k_{\ell,y,2}(y_\ell - y^*)) - A_{\ell,y} \end{bmatrix}, \tag{16}$$

with $k_{\ell,x,1}, k_{\ell,x,2}, k_{\ell,y,1}, k_{\ell,y,2} > 0$.

Note that vehicle orientations, and their respective angular velocities, have not yet been specified. Kinematically speaking, the choice of these angular velocities, and their assigned priorities, does not conflict with the fulfillment of the other tasks. On the other hand, a strict following of the angular reference for the formation orientation (γ_2) is not necessary. For these considerations, the fourth control objective defines desired orientations for the vehicles and for the formation.

Given the already defined trajectory, the desired formation orientation for the vehicles to navigate one behind the other is $\gamma_2(t) = \gamma_2^*(t) = \text{atan2}(\dot{y}^*(t), \dot{x}^*(t))$. Then, the desired vehicle orientations are given by

$$\psi_1^*(t) = \text{atan2}(\dot{y}_1^*(t), \dot{x}_1^*(t)), \text{ and } \psi_2^*(t) = \text{atan2}(\dot{y}_2^*(t), \dot{x}_2^*(t)),$$

where

$$\begin{bmatrix} x_1^*(t) \\ y_1^*(t) \end{bmatrix} = \begin{bmatrix} x^*(t) \\ y^*(t) \end{bmatrix} + \frac{d}{2\sqrt{(\dot{x}^*(t))^2 + (\dot{y}^*(t))^2}} \begin{bmatrix} \dot{x}^*(t) \\ \dot{y}^*(t) \end{bmatrix},$$

$$\begin{bmatrix} x_2^*(t) \\ y_2^*(t) \end{bmatrix} = \begin{bmatrix} x^*(t) \\ y^*(t) \end{bmatrix} - \frac{d}{2\sqrt{(\dot{x}^*(t))^2 + (\dot{y}^*(t))^2}} \begin{bmatrix} \dot{x}^*(t) \\ \dot{y}^*(t) \end{bmatrix},$$

are the desired x-y trajectories of the vehicles. In these expressions, it is assumed $d = (d_m + d_M)/2$ for simplicity.

From these definitions and from (3), the minimal norm control law to fulfill the fourth objective is given by

$$\mathbf{v}_c^{(4)} = \mathbf{J}_4^\dagger \begin{bmatrix} \dot{\gamma}_2^* - k_{\gamma_2,1} \tanh(k_{\gamma_2,2}(\gamma_2 - \gamma_2^*)) \\ \dot{\psi}_1^* - k_{\psi_1,1} \tanh(k_{\psi_1,2}(\psi_1 - \psi_1^*)) \\ \dot{\psi}_2^* - k_{\psi_2,1} \tanh(k_{\psi_2,2}(\psi_2 - \psi_2^*)) \end{bmatrix}, \tag{17}$$

where $k_{\gamma_2,1}$, $k_{\gamma_2,2}$, $k_{\psi_1,1}$, $k_{\psi_1,2}$, $k_{\psi_2,1}$, $k_{\psi_2,2} > 0$, and

$$\mathbf{J}_4 = \mathbf{J}_4(\mathbf{q}) = \begin{bmatrix} \mathbf{J}_{\gamma_2} \\ \mathbf{J}_{\psi_1} \\ \mathbf{J}_{\psi_2} \end{bmatrix}.$$

Repeating the logic given in (14), the null-space based controller for four tasks that satisfies as many tasks as possible without altering priorities is given by

$$\begin{aligned} \mathbf{v}_c = \mathbf{v}_c^{(1)} + (\mathbf{I}_8 - \mathbf{J}_1^\dagger \mathbf{J}_1)(\mathbf{v}_c^{(2)} + (\mathbf{I}_8 - \mathbf{J}_2^\dagger \mathbf{J}_2) \\ (\mathbf{v}_c^{(3)} + (\mathbf{I}_8 - \mathbf{J}_3^\dagger \mathbf{J}_3)\mathbf{v}_c^{(4)})). \end{aligned} \tag{18}$$

4.2. Conflicts between tasks

In Section 4.1 it was mentioned that tasks i and j are not in conflict if $\mathbf{C}_{ij} := \mathbf{J}_j \mathbf{J}_i^\dagger = \mathbf{0}$. In this Section, the matrices $\mathbf{C}_{ij}$ are analyzed for the cooperative payload transport problem.

If there are no obstacles nearby, then task 1 is not conflictive since $\mathbf{C}_{1j} = \mathbf{0}$ for all $j = 2, 3, 4$. Otherwise, it results

$$\mathbf{C}_{12} = \begin{bmatrix} 0 \\ 0 \\ * \end{bmatrix}, \quad \mathbf{C}_{13} = \begin{bmatrix} * \\ * \end{bmatrix}, \quad \mathbf{C}_{14} = \begin{bmatrix} * \\ 0 \\ 0 \end{bmatrix},$$

where * represents the non-null entries. These values imply conflicts between task 1 and the following tasks: trajectory tracking for the payload in the three dimensions (x, y, z), and formation orientation. These conflicts are intuitive, since the payload must deviate from the desired trajectory to avoid obstacles causing changes in the formation orientation. However, it is possible to evade obstacles and at the same time maintain the safety distance, the planned load distribution, and the vehicle orientations.

With respect to task 2, it results $\mathbf{C}_{23} = \mathbf{0}$ and $\mathbf{C}_{24} = \mathbf{0}$. Then, the fulfillment of task 2 does not condition the fulfillment of the lower priority tasks.

Finally,

$$\mathbf{C}_{34} = \begin{bmatrix} * & * \\ 0 & 0 \\ 0 & 0 \end{bmatrix},$$

which implies that the trajectory tracking for the payload in the directions (x, y) is conflictive with the formation orientation. Then, the formation orientation can not be adequately followed, but it will be satisfied in the best possible way. This is the only conflict when there are not obstacles nearby.

4.3. Stability analysis

In this Section, the stability of the proposed controller is proved under perfect velocity tracking ($\mathbf{v}_c = \dot{\mathbf{q}}$), and then, it is shown that the errors are bounded when the velocity tracking is not perfect.

Starting with task 1, from (9) and (18),

$$\mathbf{J}_1 \dot{\mathbf{q}} = \mathbf{J}_1 \mathbf{v}_c = \mathbf{J}_1 \mathbf{v}_c^{(1)} = -k_V V - \mathbf{A}_V.$$

Then, $\dot{V} + k_V V = 0$ from (8), and thus $V(t) \to 0$.

Regarding task 2, it only makes sense to analyze stability when there is no conflict with task 1, i.e., when $J_2 J_1^\dagger = \mathbf{0}$. In this case, from (13) and (18),

$$\mathbf{J}_2 \dot{\mathbf{q}} = \mathbf{J}_2 \mathbf{v}_c = \mathbf{J}_2 \mathbf{v}_c^{(2)} = \begin{bmatrix} \dot{\widetilde{d}} \\ \dot{\gamma}_{1,d} + \widetilde{\gamma}_1 \\ \dot{z}^* - k_{\ell,z,1} \tanh(k_{\ell,z,2}(z_\ell - z^*)) - A_{\ell,z} \end{bmatrix}.$$

From here, three similar analysis to those performed for task 1 should be done to obtain similar stability conditions. However, the atypical case produced by the piecewise definition of $\widetilde{d}$ is only focused. Define the energy function $\mathscr{V} = \frac{1}{2}\widetilde{d}^2$ with continuous time derivative,

$$\dot{\mathscr{V}} = \begin{cases} \widetilde{d}\dot{\widetilde{d}} & \text{if } \widetilde{d} \neq 0, \\ 0 & \text{if } \widetilde{d} = 0. \end{cases}$$

If $\widetilde{d} \neq 0$ then

$$\dot{\mathscr{V}} = \frac{-\widetilde{d} k_{d,1} k_{d,2}}{\cosh^2(k_{d,2}(d - d_*))} \mathbf{J}_d \dot{\mathbf{q}} = \frac{-\widetilde{d}^2 k_{d,1} k_{d,2}}{\cosh^2(k_{d,2}(d - d_*))} < 0,$$

where $d_* = d_m$ if $d < d_m$, or $d_* = d_M$ if $d > d_M$. Thus $\widetilde{d}(t) \to 0$.

The error convergence of the other tasks is similarly proved if there are no conflicts with higher-priority tasks, i.e., when $J_j J_i^\dagger = \mathbf{0}$ for the corresponding $j > i$.

Generally $\mathbf{v}_c \neq \dot{\mathbf{q}}$ since aerial vehicles have dynamics. Then, the error system stability requires an appropriate setting of the velocity tracking in the vehicle on-board control. However, it is proved that the errors are bounded if $\|\tilde{\mathbf{v}}\|_\infty < \infty$, where $\tilde{\mathbf{v}} := \mathbf{v}_c - \dot{\mathbf{q}}$ is the velocity tracking error.

Consider the first task of avoiding obstacles. From (8), (9) and (18),

$$\dot{V} = \mathbf{J}_1(\mathbf{v}_c - \tilde{\mathbf{v}}) + \mathbf{A}_V = -k_V V - \mathbf{J}_1 \tilde{\mathbf{v}}.$$

As the number of obstacle observations and the potential functions are bounded, it follows that $\|\mathbf{J}_1\|_\infty < \infty$, and then, $\|\mathbf{J}_1 \tilde{\mathbf{v}}\|_\infty < \infty$. Consider the energy function $\mathscr{V} = \frac{1}{2} V^2$, whose time derivative is

$$\dot{\mathscr{V}} = V\dot{V} = -k_V V^2 - V \mathbf{J}_1 \tilde{\mathbf{v}}.$$

If $k_V V > \|\mathbf{J}_1 \tilde{\mathbf{v}}\|_\infty$ then $\dot{\mathscr{V}} < 0$ implying that the potential is ultimately bounded by

$$V \leq \frac{\|\mathbf{J}_1 \tilde{\mathbf{v}}\|_\infty}{k_V}.$$

The design constant k_V and the velocity tracking error $\tilde{\mathbf{v}}$ regulate the bound and the obstacle repulsion.

Regarding task 2, again, only the bound for $\widetilde{d}$ is analyzed since the other cases are analogous. From (8), (13) and (18),

$$\mathbf{J}_d \mathbf{v}_c = \mathbf{J}_d \mathbf{v}_c^{(2)} = \dot{\widetilde{d}}.$$

In addition, $\|\mathbf{J}_d\|_\infty = 1$ from the definition of $\mathbf{J}_d$. Consider again the energy function $\mathscr{V} = \frac{1}{2}\widetilde{d}^2$. If $|\widetilde{d}| > \|\mathbf{J}_d \tilde{\mathbf{v}}\|_\infty$ then

$$\dot{\mathscr{V}} = -\frac{\widetilde{d} k_{d,1} k_{d,2}}{\cosh^2(k_{d,2}(d - d_*))} \mathbf{J}_d(\mathbf{v}_c - \tilde{\mathbf{v}}) < 0.$$

Thus

$$\left|\tanh(k_{d,2}(d-d_*))\right| = \frac{|\widetilde{d}|}{k_{d,1}} \leq \frac{\|\mathbf{J}_d\widetilde{\mathbf{v}}\|_\infty}{k_{d,1}},$$

and then, $|d-d_*|$ is ultimately bounded with the design constant $k_{d,1}$ regulating the bound value.

Similarly, it is proved that the error systems of the other tasks are bounded when there are no conflicts with higher-priority tasks. Then, task errors are bounded when there is no perfect velocity tracking, and these bounds are regulated by the controller gains. Thus, system stability depends on the correct selection of the design parameters and the correct setting of the vehicle on-board control in charge of keeping $\widetilde{\mathbf{v}}$ bounded.

4.4. Controller tuning

The obstacle avoidance requires to set the parameters a_x, a_y, a_z, n and k_V. The parameters a_x, a_y, a_z and n are defined in (6) and shape the potential fields generated by each obstacle. The higher (smaller) a_x, a_y and a_z are, the sooner (later) the cooperative avoidance task will begin, and the greater (lesser) will be the evasion maneuver. On the other hand, the higher n is, the more cubic will be the active rejection zone of each potential field. The constant k_V regulates the initial repulsion force of each potential field. Higher values of k_V produce oscillations in the control actions caused by entering and exiting the obstacle zones repeatedly. Smaller values of k_V do not provide the necessary force for vehicles to leave the avoidance zone once the obstacle is overcome. Then, intermediate values produce a safe and smooth obstacle avoidance.

The properly distribution of the load weight uses the parameters $k_{\gamma_1,1}$ and $k_{\gamma_1,2}$, which present the typical behavior of the gains of a proportional controller that includes a hyperbolic tangent. Higher values of $k_{\gamma_1,1}$ produce sudden corrections of the errors causing undesired oscillations in the weight distribution. Instead, smaller values of $k_{\gamma_1,1}$ generate slower error corrections smoothing peaks and anti-peaks produced by load pulling. On the other hand, $k_{\gamma_1,2}$ regulates the controller saturation according to the error size. Higher values of $k_{\gamma_1,2}$ saturate quickly the control actions producing an on-off controller. Instead, smaller values of $k_{\gamma_1,2}$ slow down the error corrections. Therefore, intermediate values should be considered.

The proportional gains corresponding to the other tasks have a similar behavior, and therefore, they are chosen heuristically analyzing error convergence rates and oscillations produced before the system stabilization.

The properly separation between vehicles, in addition to the proportional gains $k_{d,1}$ and $k_{d,2}$, requires to set the parameters d_m and d_M of minimum and maximum desired distance, respectively. These parameters must be geometrically analyzed according to the vehicles size, formation type, and cable lengths.

5. Simulation testbed and implementation of the kinematic formation controller

To test the control proposal in a realistic scenario, different dynamic models are incorporated in a custom software program developed in C++. The aerial vehicles are simulated using 6 DoF models of a mini-helicopter (extracted from Ref. [23]) and the cables and payload are simulated using point-like masses joined by springs and dampers for the swinging and waving motion and simple 3D solid objects for the drag. Wind and floor collision are also incorporated in the simulation testbed.

In this section, the mini-helicopter and cable models are explained in more detail along with the interconnection between them. Then the implementation of the kinematic formation controller in the simulation is described.

Table 1
Parameters of the cables and payload.

Parameters	Value
Number of cables	2
Number of masses per cable	39
Cable link mass	0.0064 [kg]
Cable diameter	0.01 [m]
Cable drag coefficient	1.0
Payload mass	1.5 [kg]
Payload edge length	0.2 [m]
Payload drag coefficient	1.05
Spring length	0.1 [m]
Spring rate	10000 [N/m]
Spring friction	0.2 [N · s/m]
Gravitational acceleration	9.7917 [m/s^2]
Air density	1.151 [kg/m^3]
Air friction	0.02 [N · s/m]
Ground repulsion	100 [N/m]
Ground friction	0.2 [N · s/m]
Ground absorption	2 [N · s/m]

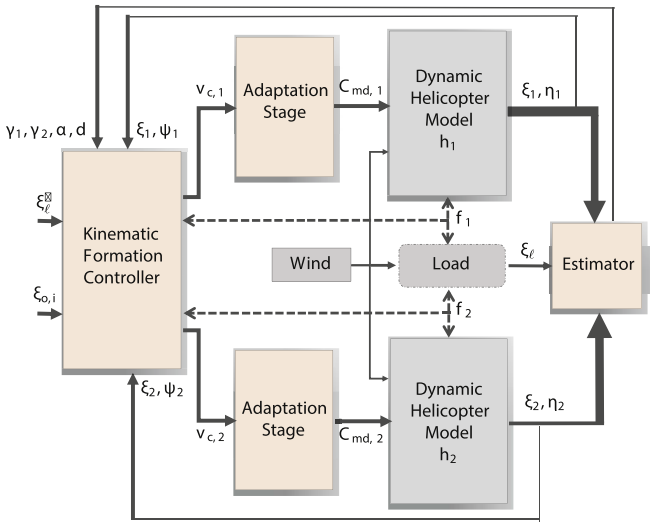

Fig. 6. Simulation testbed and kinematic formation controller framework.

5.1. Mini-helicopter dynamic model

The helicopter model used in the simulation is a very realistic nonlinear dynamic model of a small-scale helicopter given in Ref. [23]. It adequately represents the mini-helicopter dynamics in both hovering and low-speed flight envelope (up to 20 [m/ sec] forward flight). The model considers non-ideal dynamics such as flapping, drag, and actuator dynamics.

The rigid body equations of motion for the helicopter, incorporating the force and torques exerted by the load, are given by the Newton-Euler equations below,

$$\begin{aligned}
\dot{u} &= vr - wq - gs_\theta + (X_{mr} + X_{fus})/m,\\
\dot{v} &= wp - ur + gs_\phi c_\theta + (Y_{mr} + Y_{fus} + Y_{\mathrm{tr}} + Y_{vf})/m,\\
\dot{w} &= uq - vp + gc_\phi c_\theta + (Z_{mr} + Z_{fus} + Z_{ht} + Z_\ell)/m,\\
\dot{p} &= qr(I_{yy} - I_{zz})/I_{xx} + (L_{mr} + L_{vf} + L_{\mathrm{tr}} + L_\ell)/I_{xx},\\
\dot{q} &= \mathrm{pr}(I_{zz} - I_{xx})/I_{yy} + (M_{mr} + M_{ht} + M_\ell)/I_{yy},\\
\dot{r} &= pq(I_{xx} - I_{yy})/I_{zz} + (-Q_e + N_{vf} + N_{\mathrm{tr}})/I_{zz},
\end{aligned} \tag{19}$$

where u, v, w and p, q, r are the linear and angular velocities of the helicopter measured with respect to a frame attached to the helicopter g.c. (see Fig. 4).

The set of forces and moments acting on the helicopter are organized by components: $()_{mr}$ for the main rotor; $()_{\mathrm{tr}}$ for the tail rotor; $()_{fus}$

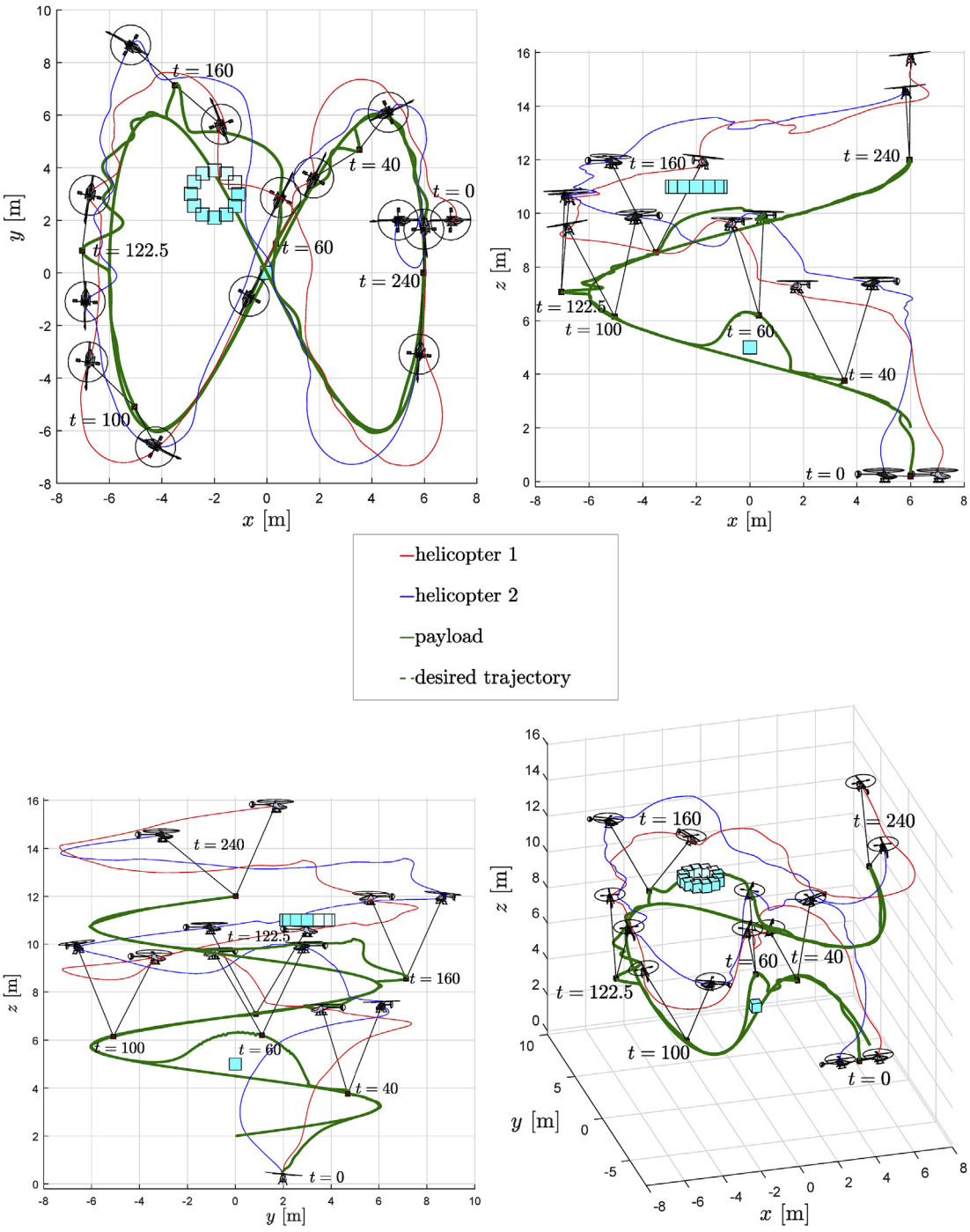

Fig. 7. Several views of the simulation results, considering obstacles avoidance and wind perturbation.

for the fuselage; $()_{vf}$ for the vertical fin; $()_{ht}$ for the horizontal stabilizer and $()_{\ell}$ for the load (cable and payload). Q_e is the torque produced by the engine to counteract the aerodynamic torque on the main rotor blades. Every component is affected by the wind as the airspeed (relative velocity between an object and the air) influences the main and tail rotor thrust and the fuselage, vertical fin and horizontal stabilizer forces (the effect of wind on the load is explained in Section 5.2). For more details on the helicopter model, see Ref. [23].

The force Z_{ℓ} and torques L_{ℓ}, M_{ℓ} (highlighted in red in (19)) are added to the original helicopter model. They are generated by the force exerted by the load (F_i) acting on a spherical joint below the helicopter g.c. (ξ_i). The force and torques are computed as follows,

$$Z_{\ell,i} = F_{w,i}, \qquad L_{\ell,i} = -F_{v,i} l_{\ell}, \qquad M_{\ell,i} = F_{u,i} l_{\ell}, \tag{20}$$

being $[F_{u,i}, F_{v,i}, F_{w,i}]^T$ the load force components expressed in the helicopter's body axes and $l_{\ell} = 0.2$ m the cable connection point distance below the g.c. of the helicopter (see Fig. 4).

The helicopter model is controlled through five input commands (C_{md}): main rotor collective and cyclic (longitudinal and lateral) blade pitch, tail rotor blade pitch and throttle; the first four inputs control the helicopter movements (up/down, back/forth, left/right, and yaw), while the last input controls the main rotor speed. The connection between these input commands (C_{md}) and the kinematic formation control law ($\mathbf{v}_c$) is made via an adaptation stage described in Section 5.3.

In the simulations, the nominal parameters of the helicopter were used which refer to MIT's X-Cell.60 acrobatic helicopter [23].

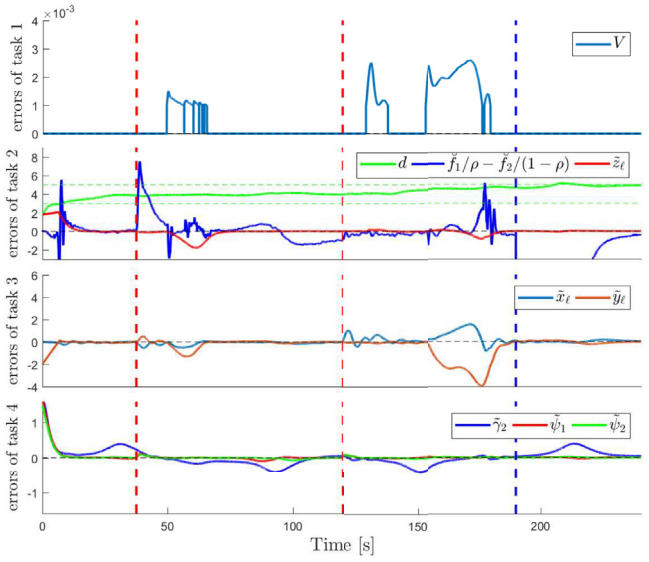

Fig. 8. Errors discriminated per task.

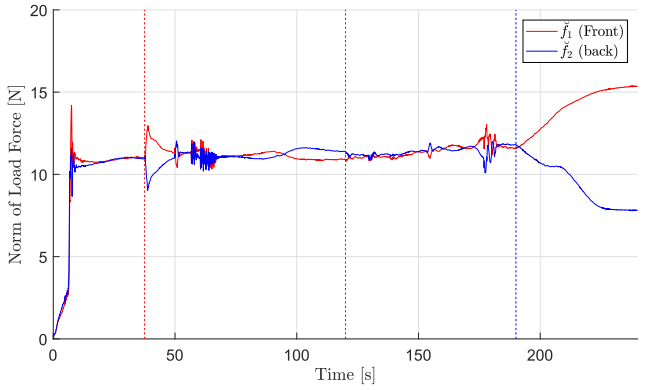

Fig. 9. Distribution of the load weight.

5.2. Flexible cable and payload dynamic models

The cables are modeled as multiple point-like masses joined by springs and dampers (Kelvin-Voigt models) to allow swinging and waving movements. Each cable comprises thirty-nine point-like masses, where the first mass is attached to a spherical joint below the helicopter g.c (see Fig. 4). and the last mass is connected to a special point-like mass (payload) common to every cable as indicated in Fig. 5. Each mass is affected by the elastic and viscous force generated by the surrounding springs and dampers, the gravitational force, air friction force, drag force and other ground related forces (friction, absorption and repulsion).

The number of links in the cable is set according to the desired detail level; in a four meters cable, the forty links (thirty-nine masses plus payload) give a resolution of ten centimeters in the cable's movement. The springs that join each pair of masses (including the payload) are all equal; with a specific length, friction constant and very high rate to avoid stretching the cable. Others parameters affect the interaction between the cables/payload and the ground. In addition, the air density and air friction constant are also included in the simulation. The effect of drag and wind on the cable links and payload are simulated according to the following formula,

$$F_d = \frac{1}{2}\rho v^2 c_d A, \tag{21}$$

where ρ is the air density, v is the velocity with respect to air, A is the cross-sectional area, and c_d is the drag coefficient. Every link is treated as a solid cylinder and the payload as a solid cube to calculate the cross-sectional area, each with its corresponding drag coefficient.[1] In Table 1 there is a list of all the parameters used in the simulation.[2]

The following link shows a detailed video related to the dynamic evolution of the cable and the transported payload: https://www.youtube.com/watch?v=7kgfY9xIgmc. Note that the wind perturbation as well as the load weigh distribution between helicopters (f_1 and f_2) have been considered.

5.3. Implementation of the kinematic formation controller

To let the helicopters track the corresponding flight commands $\mathbf{v}_c = [\mathbf{v}_{c,1}^T, \mathbf{v}_{c,2}^T]^T$, $\mathbf{v}_{c,i} = [\dot{x}_{i,c}, \dot{y}_{i,c}, \dot{z}_{i,c}, \dot{\psi}_{i,c}]^T$, the adaptation stage depicted in Fig. 6 is added to each vehicle. This stage is composed by two steps: a velocity frame change and a PID-based cascade control. In the first step, the flight commands $\mathbf{v}_{c,i}$ are rotated using ψ_i to be expressed in a frame attached to the i-th helicopter but without roll and pitch movements. Then, the PID architecture generates the servo signal inputs $C_{md,i}$ (see details in Refs. [24,25]).

Fig. 6 exposes the flexibility of this kinematic based controller. Modifying only the adaptation stage it is possible to use the same controller for other types of miniature rotorcraft, e.g., using the PID Adaptation Stage of [26] the kinematic formation controller can be applied to quadrotors.

The cables and payload simulations are implemented in a custom C++ program, along with the mini-helicopter models and adaptation stages.[3] In this program, the cables/payload system and each mini-helicopter/adaptation stage run in separated threads synchronized using events. On the other hand, the kinematic controller is programmed in MATLAB® (The MathWorks Inc., Massachusetts, USA) and continuously communicates with the C++ program through shared memory. That is, the MATLAB code reads the state of each mini-helicopter and cable/payload from the shared memory, executes the kinematic controller, and then writes the control actions for each vehicle into the shared memory. The C++ program reads these control actions, calculates the servo signals for the mini-helicopter inputs, simulates the dynamic models and then writes the states into the shared memory. The formation controller update rate is 60 Hz and the adaptation stage update rate is 500 Hz. The dynamic models of the mini-helicopters, cables and payload are simulated using a fourth-order Runge-Kutta method with an integration step size of 0.001 s.

6. Simulation results

In this Section, simulation results are presented to validate the controller performance in a realistic simulation environment. It is simulated setting 60 sampling periods per second.

It is well known that following an upward eight-way trajectory is a complicated task that can be used to efficiently evaluate the controller performance. Therefore, the reference trajectory chosen to perform the first simulations is given by

$$\xi_\ell(t) = \begin{bmatrix} r\cos(2\pi t/T) \\ r\sin(4\pi t/T) \\ 2 + 10t/T \end{bmatrix},$$

where $T = 240$sec is the total time of simulation, and $r = 6$ m regulates

[1] The cross-sectional area of the payload and cable are considered constant, equal to the cube face area and cylinder lateral area, respectively.

[2] The air friction and ground repulsion, friction and absorption constants are scaled up for the payload according to difference in mass and cross-sectional area between the payload and a cable link.

[3] the flexible cable implementation was inspired by the NeHe OpenGL rope physics tutorial at http://nehe.gamedev.net/tutorial/rope_physics/17006/, and the mini-helicopter model is a custom C++ implementation of the equations found in Ref. [23].

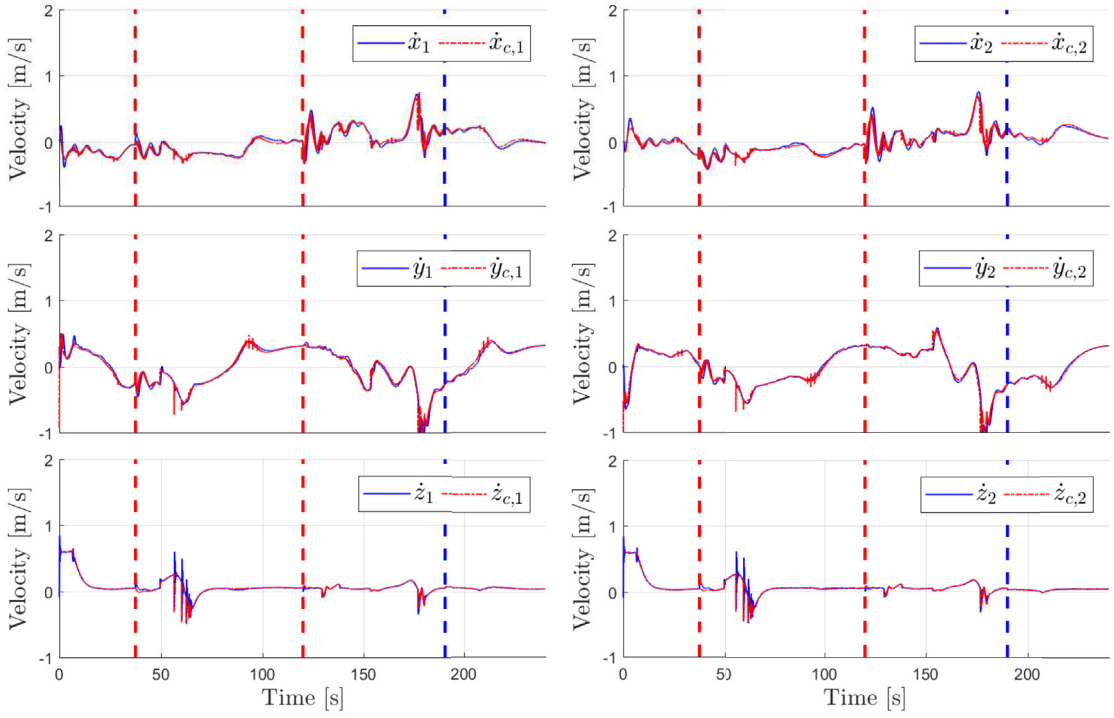

Fig. 10. Velocity commands as calculated by the kinematic controller and the actual velocities of each helicopter.

the scale of the eight-way trajectory. The design constants of the kinematic controller for the payload to follow this trajectory are: $k_{\ell,x,1} = k_{\ell,y,1} = k_{\ell,z,1} = 0.75$, and $k_{\ell,x,2} = k_{\ell,y,2} = k_{\ell,z,2} = 0.475$. The payload mass is 1.75 kg, it hangs from 4 m long cables tied to the helicopters. The load weight (approximately 2 kg in total) is evenly distributed between the vehicles ($\rho = 0.5$), except in the last 50sec where it is desired that the vehicle ahead carries twice the weight of the vehicle behind $\rho = 2/3$. For this task, it is set $k_{\gamma_1,1} = 0.01$, $k_{\gamma_1,2} = 0.2$, and a sliding-window of length 60 sampling periods (1sec).

The initial positions of the vehicles are $\xi_1 = [7,2,0.25]^T$ and $\xi_2 = [5,2,0.25]^T$, the initial orientations are $\psi_1 = \psi_2 = 0$, and the initial position of the payload is $\xi_\ell = [6, 2, 0]^T$. The range of safe distance between the vehicles is [3,5] meters, and the design constants from (11) to reach this objective are $k_{d,1} = 0.5$ and $k_{d,2} = 0.75$. The remaining design constants of the kinematic controller are $k_{\gamma_2,1} = 0.5$, $k_{\gamma_2,2} = 0.75$, $k_{\psi_1,1} = k_{\psi_2,1} = 0.5$ and $k_{\psi_1,2} = k_{\psi_2,2} = 0.75$.

With the purpose of showing the wind influence, a constant wind of 5.5 m/sec is considered, whose direction points to the positive x-axis. The wind starts at time $t = 37.5$sec and ends at time $t = 120$sec. The rest of the time the wind is removed. In addition, two obstacles (one static and the other dynamic) are placed in the simulation environment with positions given by

$$\xi_{o,1} = \begin{bmatrix} 0 \\ 0 \\ 5 \end{bmatrix}, \text{ and } \quad \xi_{o,2}(t) = \begin{bmatrix} r_2 \cos(20\pi t/T) \\ r_2 \sin(20\pi t/T) \\ 11 \end{bmatrix},$$

where $r_2 = 0.9$ m is the turning radius of the dynamic obstacle. The distance from which the obstacles are detected is regulated by the parameters of the potential fields (6), which are set in $a_x = a_y = a_z = n = 2$ and $\varsigma = 0.001$. Increasing $a_x = a_y = a_z$ or decreasing ς implies delaying the start of the avoidance. The repulsion force is regulated by the design constant of (9), which is set in $k_V = 0.1$. This configuration produces a safe and smooth obstacle avoidance.

Different views of the helicopters, payload and obstacle trajectories are shown in Fig. 7. The control errors of the simulation are displayed in Fig. 8. The cable and payload positions and the helicopter postures at times $t = 0$, 40, 60, 100, 122.5, 160, 240sec are also plotted in Fig. 7. The norm of the forces made by each vehicle is shown in Fig. 9.

The wind is suddenly introduced at time $t = 37.5$ (see the first red vertical line in Figs. 8 and 9), producing oscillations in the formation (see formation at $t = 40$ in Fig. 7). The static obstacle is detected at $t = 49.6$ (see plot of V in Fig. 8), and the formation avoids it smoothly from above (see formation at $t = 60$ in Fig. 7). The force signals present peaks and anti-peaks produced by load pulling, which are caused by several factors such as: wind, turning, obstacle avoidance, accelerations, etc. The wind disturbs the force balance reached by the vehicles (see the first red vertical line in Fig. 9). During the avoiding task, the errors in trajectory tracking and formation orientation increase since these tasks have conflicts with task 1 (see Section 4.2). A trajectory tracking error is observed at $t = 100$ because the formation rotates and the wind influences perpendicularly. A new formation oscillation is caused by the sudden removal of the wind at $t = 120$ (see the second red vertical line in Figs. 8 and 9). The dynamic obstacle is detected at $t = 128.9$ and then at $t = 153.3$. At the first opportunity the formation moves backwards because the obstacle is directed towards the formation (see formation at $t = 122.5$ in Fig. 7). Subsequently, the dynamic obstacle is evaded by its side (see formation at $t = 160$ in Fig. 7). Finally, the load weight is modified at $t = 190$, producing a transition error in the task 3 (see blue vertical line in Fig. 8). The other task are not influenced by this process. The vehicle behind navigates a little higher to distribute evenly the load weight. The vehicle ahead finishes the simulation navigating higher, since it must transport two thirds of the load weight from $t = 190$ (see yz-view in Fig. 7). The vehicles correct its separation only when it is not within the allowed range. The errors of tasks 3 and 4 are small except in curves where dynamic effects and the realistic model of the cable introduce oscillations that difficult the complete fulfillment of the formation orientation task evidencing the conflict between these tasks (see Section 4.2). A video of the simulation can be seen in https://www.youtube.com/watch?v=nIvKE2iCoRQ.

Fig. 10 shows the velocities (control actions) calculated by the kinematic controller $\mathbf{v}_{c,i} = [\dot{x}_{c,i}, \dot{y}_{c,i}, \dot{z}_{c,i}, \dot{\psi}_{c,i}]$ and the actual velocities of

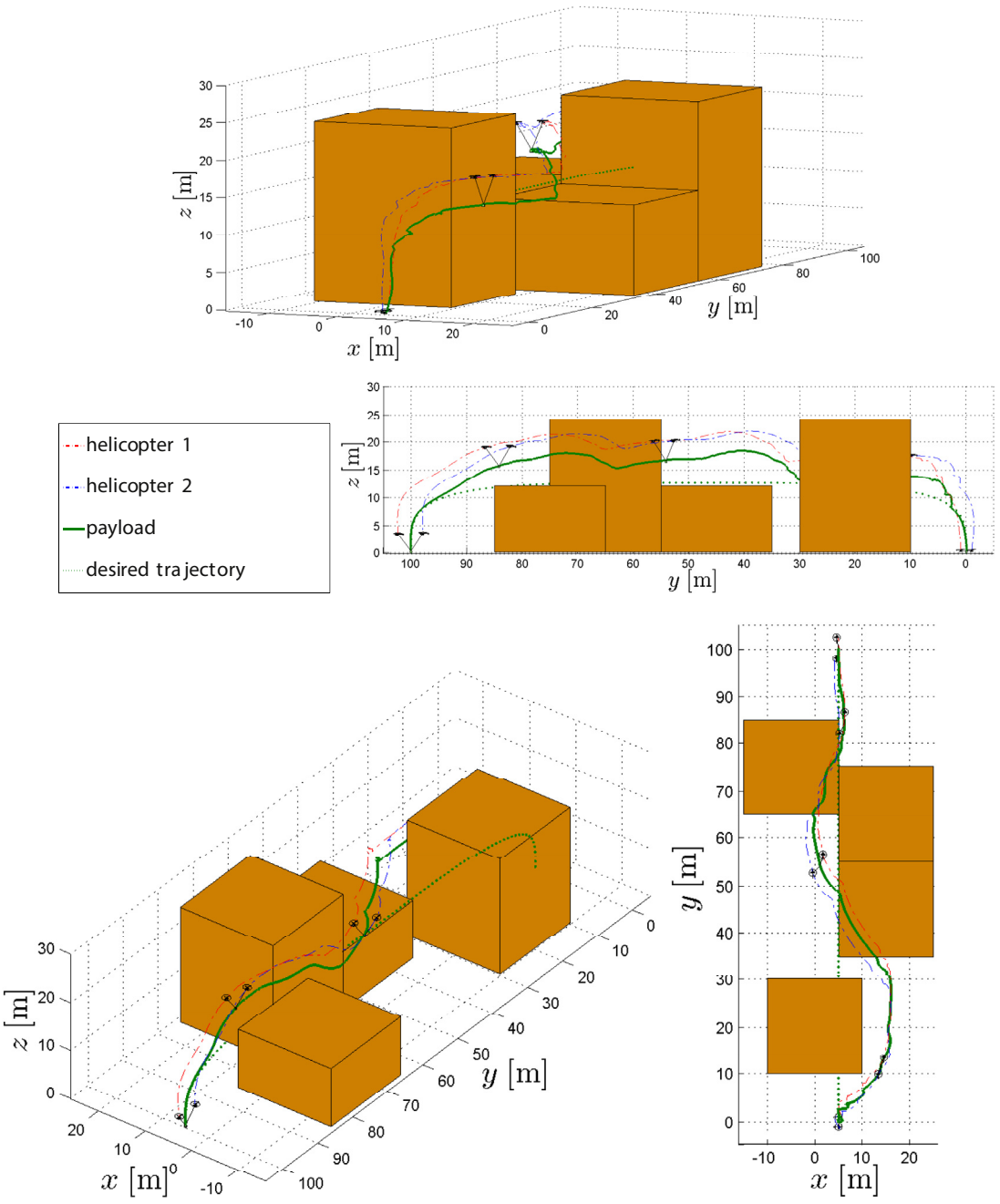

Fig. 11. Several views of the simulation environment.

each helicopter in the global frame. The PID adaptation stage has been conveniently adjusted and a good tracking is achieved. The curves present any picks caused by occasional exits from areas with $V > 0$ during evasion (see plot of V in Fig. 8), which are smoothed by the PID internal loop.

Finally, a realistic environment is simulated in which two vehicles carry a payload from one point to another avoiding buildings and distributing evenly the load weight ($\rho = 0.5$). With the purpose of calculating the collision potential V, the building walls are sub-sampled and fixed obstacles are generated in these places. Several views of the simulation result are shown in Fig. 11. The desired load trajectory is plotted in green dotted line, and the actual load trajectory is plotted in green solid line. In addition, the trajectories followed by the helicopters are shown in dash-dot lines. The initial point of the load is $\xi_\ell = [5, 0, 0]^T$ and the final point is $\xi_\ell = [5, 100, 0]^T$. A constant wind of 5.5 m/sec with positive x-axis direction is simulated. The wind affects the formation during the whole simulation, except when it passes by the side of the first building that blocks the wind. Note that the vehicles carry the load in an appropriate manner arriving at destination in time and in due form. A video of the simulation can be seen in https://www.youtube.com/watch?v=SLCsHZz4uTA.

Exhaustive simulations were carried out to analyze the wind effects on the formation. For these particular mini-helicopter, cable and payload models, and design constants, the tracking errors are large when the wind speed is greater than 40 km/h (strong breeze in the Beaufort wind force scale). However, increasing the payload mass and/or modifying some design constants, the system can better handle winds of up to 60 km/h (high wind in the Beaufort wind force scale).

7. Conclusions

In this paper, a novel multi-objective controller is proposed in order to carry a payload via flexible cables with two rotorcraft UAVs through a desired trajectory. The control proposal is based on null-space theory considering wind disturbance, static and dynamic obstacle avoidance, as well as properly distribution of the load weight according to factors such as onboard energy availabilities or carrying capacities. Besides, the stability of the proposed kinematic control law is proven by using of Lyapunov theory. Accurate dynamic models of a mini-helicopter and a cable-suspended payload are considered to generate a realistic test scenario. The kinematic control approach is very flexible since it can be used for another type of aircraft by changing only the adaptation stage described in Fig. 6.

Figures and videos of the simulations show the good performance of the proposed controller. The tasks were completed according to their pre-established priorities reducing as much as possible the conflicts between them. The incorporation of the dynamic model of the helicopter and the load in the simulations, allows a very fine adjustment of the kinematic controller parameters reducing the gap between simulation and experimentation.

References

[1] Andrade R, Raffo GV, Normey-Rico JE. Model predictive control of a tilt-rotor UAV for load transportation. European control conference (ECC), Aalborg, Denmark. 2016.

[2] Potter JJ, Adams CJ, Singhose W. A planar experimental remote-controlled helicopter with a suspended load. IEEE ASME Trans Mechatron 2015;20(5):235–47.

[3] Zürn M, Morton K, Heckmann A, McFadyen A, Notter S, Gonzalez F. MPC controlled multirotor with suspended slung Load: system architecture and visual load detection. IEEE Aerospace conference, Montana, USA. 2016.

[4] Masone C, Bülthoff HH, Stegagno P. Cooperative transportation of a payload using quadrotors: a reconfigurable cable-driven parallel robot. IEEE/RSJ international conference on intelligent robots and systems (IROS), Daejeon, Korea. 2016.

[5] Palunko I, Cruz P, Fierro R. Agile load transportation: safe and efficient load manipulation with aerial robots. IEEE Robot Autom Mag 2012;19(3):69–79.

[6] Mattei M, Scordamaglia V. Task priority approach to the coordinated control of a team of flying vehicles in the presence of obstacles. IET Contr Theory & Appl 2012;6(13):2103–10.

[7] Raffo GV, de Almeida MM. Nonlinear robust control of a quadrotor UAV for load transportation with swing improvement. American control conference (ACC), Boston, USA. 2016.

[8] Alothman Y, Gu D. Quadrotor transporting cable-suspended load using iterative linear quadratic regulator (iLQR) optimal control. Computer science and electronic engineering conference (CEEC), Colchester, England. 2016.

[9] de Crousaz C, Farshidian F, Buchli J. Aggressive optimal control for agile flight with a slung load. Workshop on machine learning in planning and control of robot motion, Chicago, USA. 2014.

[10] Cruz PJ, Oishi M, Fierro R. Lift of a cable-suspended load by a quadrotor: a hybrid system approach. American control conference, Chicago, USA. 2015.

[11] Sreenath K, Lee T, Kumar V. Geometric control and differential flatness of a quadrotor UAV with a cable-suspended load. IEEE 52nd annual conference on decision and control (CDC), Firenze, Italy. 2013.

[12] Lee H, Kim HJ. Estimation, control, and planning for autonomous aerial transportation. IEEE Trans Ind Electron 2017;64(4):3369–79.

[13] Jiang Q, Kumar V. The inverse kinematics of cooperative transport with multiple aerial robots. IEEE Trans Robot 2013;29(1):136–45.

[14] Michael N, Fink J, Kumar V. Cooperative manipulation and transportation with aerial robots. Aut Robots 2011;30(1):73–86.

[15] Lee T. Geometric control of quadrotor UAVs transporting a cable-suspended rigid body. IEEE Trans Contr Syst Technol. 2018;26(1):255–64.

[16] Estevez J, Lopez-Guede JM, Graña M. Particle swarm optimization quadrotor control for cooperative aerial transportation of deformable linear objects. Cybern Syst 2016;47(1–2):4–16.

[17] Estevez J, Graña M, Lopez-Guede JM. Online fuzzy modulated adaptive PD control for cooperative aerial transportation of deformable linear objects. Integrated Comput Aided Eng 2017;24(1):41–55.

[18] Babaie R, Ehyaie AF. Robust optimal motion planning approach to cooperative grasping and transporting using multiple UAVs based on SDRE. Transactions of the Institute of Measurement and Control; 2016. p. 1–18.

[19] Fink J, Michael N, Kim S, Kumar V. Planning and control for cooperative manipulation and transportation with aerial robots. Int J Robot Res 2011;30(3):324–34.

[20] Maza I, Kondak K, Bernard M, Ollero A. Multi-uav cooperation and control for load transportation and deployment. J Intell Rob Syst 2010;57(1–4):417–49.

[21] Energy evaluation of low-level control in UAVs powered by lithium polymer battery. ISA (Instrum Soc Am) Trans 2017;71:563–72.

[22] Antonelli G, Arrichiello F, Chiaverini S. The null-space-based behavioral control for autonomous robotic systems. Intell Serv Robot 2008;1(1):27–39.

[23] Gavrilets V. Autonomous aerobatic maneuvering of miniature helicopters PhD. thesis Cambridge, MA: Massachusetts Institute of Technology. Dept. of Aeronautics and Astronautics; 2003.

[24] Salinas LR, Slawiñski E, Mut VA. Kinematic nonlinear controller for a miniature helicopter via lyapunov techniques. Asian J Contr 2014;16(3):856–70.

[25] Gandolfo D, Salinas L, Brandão A, Toibero M. Path following for unmanned rotorcraft - an approach on energy autonomy improvement. Inf Technol Contr 2016;45(1):87–98.

[26] Gandolfo DC, Salinas LR, Brandão A, Toibero JM. Stable path-following control for a quadrotor helicopter considering energy consumption. IEEE Trans Contr Syst Technol 2017;25(4):1423–30.